Published in final edited form as:

J Physiol. 2020 January ; 598(1): 189–205. doi:10.1113/JP278612.

Differential impact of two critical respiratory centers in opioid-induced respiratory depression in awake mice

Adrienn G. Varga[1,2], **Brandon T. Reid**[1], **Brigitte L. Kieffer**[3], **Erica S. Levitt**[1,2]

[1]Department of Pharmacology and Therapeutics, University of Florida, Gainesville, FL 32610

[2]Center for Respiratory Research and Rehabilitation, Department of Physical Therapy, University of Florida, Gainesville, FL 32610

[3]Douglas Research Centre, McGill University, Montreal, QC, Canada

Abstract

The primary cause of death from opioid overdose is respiratory failure. High doses of opioids cause severe rate depression and increased risk of fatal apnea, which correlate with increasing irregularities in breathing pattern. Mu opioid receptors (MORs) are widely distributed throughout the brainstem respiratory network, but the mechanisms underlying respiratory depression are poorly understood. The medullary pre-Bötzinger complex (preBötC) and the pontine Kölliker-Fuse nucleus (KF) are considered critical for inducing opioid-related respiratory disturbances. We used a conditional knockout approach to investigate the roles and relative contribution of MORs in KF and preBötC neurons in opioid-induced respiratory depression in awake adult mice. The results revealed dose-dependent and region-specific opioid effects on the control of both respiratory rate and pattern. Respiratory depression induced by an anti-nociceptive dose of morphine was significantly attenuated following deletion of MORs from either the KF or preBötC, suggesting cumulative network effects on respiratory rate control at low opioid doses. Deletion of MORs from KF neurons also relieved rate depression at near-maximal respiratory depressant doses of morphine. Meanwhile, deletion of MORs from the preBötC had no effect on rate following administration of high doses of morphine. Instead, a severe ataxic breathing pattern emerged with many apneas. We conclude that opioids affect distributed areas of the respiratory network and opioid-induced respiratory depression cannot be attributed to only one area in isolation. However, countering the effects of near maximal respiratory depressant doses of opioids in the KF may be a powerful approach to combat opioid overdose.

Introduction

The opioid epidemic is a U.S. public health crisis (Rudd *et al*., 2016; Volkow & Collins, 2017). Opioids exert deleterious and potentially fatal effects on respiration by activating mu opioid receptors (MORs; Dahan et al., 2001, 2010; Pattinson, 2008). Despite the negative

Correspondence to: Dr. Erica S. Levitt, erica.levitt@ufl.edu, University of Florida, 1200 Newell Drive, Gainesville, FL 32610.
Author contributions: A.G.V. and E. S. L. designed research; A. G. V., E. S. L. and B. T. R. performed experiments; A. G. V. and E. S. L. analyzed data; B.L.K. contributed reagents; A.G.V, B.T.R. and E.S.L. wrote the manuscript; A.V.G, B.L.K. and E.S.L. edited the manuscript.

Conflict of Interest: The authors declare no competing financial interests.

impact on breathing, opioid agonists, such as morphine, remain the most frequently prescribed painkillers due to their potent analgesic effects, which are also mediated by MORs at multiple sites of the central and peripheral nervous system (Yaksh, 1997; Yaksh *et al.*, 2015). While the neural pathways mediating opioid analgesia are extensively characterized, the neural correlates and mechanisms of opioid-induced respiratory disturbances are unclear (Lalley et al., 2014; Montandon and Horner, 2014).

The main cause of death from opioids is respiratory rate depression and a subsequent cessation of breathing. Interestingly in these cases, the advancement from normal breathing to apnea is not a progressively stable slowing of rate. Instead, severe rate depression and a higher risk of fatal apnea are correlated with increasing irregularities in the breathing pattern (Bouillon *et al.*, 2003; Pattinson, 2008).

While MORs are distributed throughout the brainstem respiratory network (Mansour et al., 1994; Lonergan et al., 2003), the medullary pre-Bötzinger complex (preBötC) and the pontine Kölliker-Fuse nucleus (KF) are considered critical for inducing opioid-related respiratory disturbances (Lalley, 2003; Mustapic *et al.*, 2010; Montandon *et al.*, 2011, 2016; Prkic *et al.*, 2012; Lalley *et al.*, 2014; Montandon & Horner, 2014; Levitt *et al.*, 2015; Stucke *et al.*, 2015). The preBötC inspiratory rhythm generator contains a subpopulation of neurons that express MORs which have been implicated in opioid-induced respiratory rate suppression both *in vitro* and *in vivo* (Gray et al., 1999; Montandon et al., 2011; Montandon 2016). Additionally, opioid-induced patterns referred to as ‘quantal breathing’ have been linked to skipped cycles of inspiratory output from the preBötC (Mellen et al., 2003). The main source of quantal breathing is likely the opioid-induced imbalance of preBötC rhythmic activity and the activity of a rate-modulating input, the mechanism of which is not clear (Feldman *et al.*, 2003; Mellen *et al.*, 2003; Janczewski & Feldman, 2006; Wittmeier *et al.*, 2008; Lal *et al.*, 2011; Baesens & MacKay, 2013).

While medullary networks are responsible for rhythm generation, the KF is necessary for stabilizing the respiratory rate and generating a normal “eupneic” respiratory pattern (St.-John & Paton, 2004; Dutschmann & Dick, 2012; Dhingra *et al.*, 2017; Ramirez & Baertsch, 2018). Application of an opioid agonist into the KF area results in the reduction of respiratory rate accompanied by changes in pattern (Hurlé et al., 1985; Prkic et al., 2012; Levitt et al., 2015). Notably, a limiting factor in prior studies defining how neurons in each respiratory nucleus contribute to respiratory depression is that local application of opioid agonists or antagonists not only affect the local somatodendritic MORs, but also the MORs on local presynaptic terminals, while leaving receptors on terminals in projection regions unaffected. This is especially an issue when attempting to separate the role of the KF and preBötC, since they are reciprocally connected and directly influence each other (Ezure & Tanaka, 2006; Tan *et al.*, 2010; Song *et al.*, 2012; Yokota *et al.*, 2015; Geerling *et al.*, 2017; Yang & Feldman, 2018).

To overcome this limitation, and to further our understanding of how MORs contribute to respiratory disturbances, we used a genetic approach to conditionally delete MORs both from the somatodendritic local areas and terminals in projection regions, while leaving presynaptic MORs intact. $MOR^{fl/fl}$ mice were used to selectively ablate MORs from either

KF or preBötC neurons via virally-mediated bilateral expression of Cre recombinase. Our results provide a direct comparison of the significance of MORs in the KF and the preBötC in morphine-induced respiratory disturbances. Importantly, our data indicate that activation of both preBötC and KF MORs contribute to respiratory rate depression at lower, anti-nociceptive doses of morphine, whereas, activation of MORs located in the KF is more detrimental to the rate and stability of the respiratory pattern than MORs in the preBötC following high-dose morphine. Together, these data contribute to our understanding of the mechanisms underlying opioid-induced respiratory disturbances.

Materials and Methods

Ethical approval

Homozygous mice (male and female, 4–6 months old) with a floxed mu opioid receptor gene ($MOR^{fl/fl}$) (Weibel *et al.*, 2013) or wild-type C57/129 counterparts were used for all experiments. Mice were bred and maintained at the University of Florida or Oregon Health & Science University animal facility. Mice were group-housed in standard sized plastic cages and kept on a 12-hour light/dark cycle, with water and food available *ad libitum*. All procedures conducted were in accordance with the National Institutes of Health guidelines and with approval from the Institutional Animal Care and Use Committees of the Oregon Health & Science University or the University of Florida (approval reference number 201609515), and conform to the principles and regulations as described by Grundy (2015).

Stereotaxic injections and viruses

Mice were anesthetized with isoflurane (2–4% in 100% oxygen, Zoetis) and mounted in a stereotaxic frame (Kopf Instruments, Tujunga, CA) where anesthesia was maintained through a nose cone. The dorsal skull was exposed and levelled horizontally between bregma and lambda. A small craniotomy was made to access either the KF (y = −5 mm, x = ±1.7 mm, from bregma) or the preBötC (y = −7 mm, x = ±1.3 mm, from bregma), bilaterally. A glass micropipette filled with either AAV2-CMV-Cre-GFP or AAV2-CMV-GFP virus (obtained from UNC Vector Core) was lowered into the KF (z = −3.9 mm) or the preBötC (z = −5.625 mm). Virus was injected (5 × 10 nl per side) with a Nanoject III (Drummond Scientific Company, Broomall, PA, USA) over the course of 2.5 min. Following injection, the pipette was left in place for 10 min and slowly retracted. The wound was closed with Vetbond tissue adhesive (3M Animal Care Products, St. Paul, MN, USA). Mice received meloxicam (5 mg/kg in saline, s.c.), were placed in a recovery chamber and kept warm until they ambulated normally. Experiments (electrophysiology, plethysmography and immunohistochemistry) were performed 4–5 weeks later.

Placement of injections was verified in brain slices (50–100 μm or 230 μm) from every mouse by visualizing GFP fluorescence using a multizoom microscope (Olympus MVX10 or Nikon AZ100). Injection sites were considered acceptable if the maximal intensity and spread of GFP coincided with the KF (rostro-caudally −5.3 to −4.8 mm from bregma) or preBötC (rostro-caudally −7.1 to −6.8 mm from bregma) in both hemispheres. Injections targeting the KF were centered at the tip of the superior cerebellar peduncle (scp) when the peduncle was elongated and diagonally oriented. The dorsal-ventral boundaries of infection

were contained between the external lateral parabrachial nucleus and ~500 μm ventral to the tip of the scp (3.7 to 4.25 mm ventral from bregma; Figure 1 A, E). Injections targeting the preBötC were centered ventral to the nucleus ambiguous in the ventral lateral medulla. The rostral-caudal boundaries of infection were contained in coronal slices with highly laminar inferior olives (Figure 1 C, F).

Mice with AAV2-CMV-Cre-GFP injected in the KF or preBötC will be referred to as “KF MOR-cKO” and “preBötC MOR-cKO”, respectively. Mice receiving AAV2-CMV-GFP control injections into the KF or preBötC will be referred to as “KF-GFP” and “preBötC-GFP”, respectively.

Plethysmography

Head-out plethysmography was used to measure the instantaneous respiratory rate of awake mice 4–5 weeks following viral injections (Mortola & Noworaj, 1983; Levitt *et al.*, 2013). Briefly, individual mice were administered saline (10 μl/g, i.p.) or morphine sulfate (one of three doses: 10, 30 or 100 mg/kg in saline, i.p.) and placed into a 65-ml chamber with their heads protruding through a flexible, airtight neck collar into the head chamber. The head chamber was ventilated with a constant airflow (0.7 L/min). Respiratory measurements were obtained from a pneumotachograph connected to the body chamber and a volumetric pressure transducer (Grass Instrument Co., West Warwick, RI, USA), amplified with a Transbridge 4M amplifier (WPI, Sarasota, FL, USA) and digitized with PowerLab 2/26 in Lab Chart 8 (AD Instruments, Colorado Spring, CO, USA). In pilot experiments, mice were handled and exposed to the plethysmograph daily for 4–7 days leading up to the experiment. This did not change respiratory parameters measured during the saline or morphine trials and thus such an acclimation paradigm was discontinued.

All plethysmography experiments were carried out at room temperature without thermoregulatory compensation. Each mouse was administered saline first and then placed in the plethysmograph for 45 min. Following the saline trial, mice were placed in their home cages for at least 45 min before administration of morphine and returned to the plethysmograph for 45 min. Plethysmography experiments were carried out in two phases. In the first phase, KF MOR-cKO, KF-GFP, preBötC MOR-cKO and preBötC-GFP mice were injected with saline followed by a 10 mg/kg dose of morphine (anti-nociceptive or “low-dose”;Weibel et al., 2013). In the second phase, a new cohort of mice (KF MOR-cKO, KF-GFP, preBötC-Cre MOR-cKO, preBötC-GFP mice) were injected with saline followed by a 30 or 100mg/kg dose of morphine (medium and high doses; Dahan et al., 2001; Romberg et al., 2003). The doses of morphine were pseudo-randomized and blinded to the experimenter. The same mice were retested with the other dose of morphine 7–10 days later to avoid the development of tolerance. All phases of experiments also included naïve littermate control mice that did not receive any viral injection. The saline trial served as an internal vehicle control for each mouse. Respiratory rates during repeated saline experiments were not different ($p > 0.05$ with paired two-tailed t-test).

Plethysmography data analysis

Plethysmography data were processed offline with Lab Chart 8 and exported into Microsoft Excel. Representative segments of the continuous 45 min long respiratory trace were analyzed in one minute bins to obtain the average respiratory rate (breaths per minute). Summary graphs represent the steady-state respiratory rate, which was determined by averaging respiratory rate during the time period of 25–40 minutes (peak effect of morphine). Steady-state respiratory rate following morphine was normalized to steady-state respiratory rate following saline for each animal ("within subject"). The normalized morphine-induced respiratory rate was then averaged across animals for comparisons between groups.

Respiratory pattern analyses, such as rate variability, respiratory phase durations and apnea counts were performed in Spike2 (CED, Cambridge, England) with custom written scripts. To quantify the amount of variability of the instantaneous respiratory rate caused by morphine, the inter-breath interval values between 25–40 minutes were extracted in 10 ms bins. Respiratory variability was assessed by calculating the coefficient of variation (CV %) for each respiratory cycle. The CV% was defined as the ratio of the standard deviation of the instantaneous respiratory frequency to the mean instantaneous frequency, and expressed as a percentage. Representative example Poincaré plots of T_{Tot} for the n^{th} respiratory cycle vs. T_{Tot} for the $n^{th}+1$ cycle were also plotted to illustrate the variability of T_{Tot}.

Analysis of respiratory phase durations (inspiration: T_i; expiration: T_e) was based on representative 1 min periods in the steady-state phase of the saline and morphine (10 mg/kg) trials. Experiments with higher doses of morphine were not analyzed for T_i and T_e due to the increased variability in respiratory patterns and thus lack of 'representative periods' (see Results).

Apnea counts were obtained from the entire 45 min of each respiratory recording. Apneas were defined as pauses between breaths that lasted longer than 1 s (Levitt *et al.*, 2013). The results of automated apnea count were manually inspected to ensure that events were accurately detected.

Immunohistochemistry

Following plethysmography, mice were deeply anesthetized with isoflurane (Zoetis) and either transcardially perfused with PBS followed by 10% formalin, or decapitated without perfusion. In both cases the brains were removed and cryoprotected in 10% formalin/30% sucrose solution at 4°C before further processing. Serial coronal sections (40–100 μm) were cut using a vibratome (Leica VT 1200S) or a microtome. The free-floating sections were then stained for specific neuronal markers for cell counting (NeuN) and verification of appropriate injection sites (somatostatin in the preBötC). First, sections were rinsed in tris-buffered saline (TBS), then washed in diluting buffer (TBS containing 2% BSA, 0.4% TritonX-100, 1% filtered NGS) for 30 minutes. The sections were blocked in 20% NDS in TBS for 30 minutes to reduce nonspecific staining and immediately incubated in primary antibody for 24 hours (mouse monoclonal anti-NeuN [Millipore MAB377] 1:1000 in diluting buffer) or 48 hours (mouse monoclonal anti-somatostatin [Santa Cruz Biotech

sc-74556] 1:200 in diluting buffer) at 4°C. GFP was amplified using anti-GFP rabbit monoclonal antibody with Alexa Fluor 488 conjugate (ThermoFisher, 1:1000 in diluting buffer). Following incubation, sections were washed in diluting buffer and incubated in secondary antibody at room temperature for 2 hours (goat anti-mouse IgG Alexa Fluor Plus 555, 1:1000 in diluting buffer). The sections were washed in TBS, rinsed once in ddH_2O, then serially mounted with Fluoromount-G DAPI (ThermoFisher) mounting medium. Images were collected on a confocal laser scanning microscope (Nikon A1R) with a 10× objective (N.A. 0.3) and a multizoom microscope (Nikon AZ100) with a 1× objective (N.A. 0.1) and processed in Fiji (Schindelin *et al.*, 2012).

Brain slice electrophysiology

The functional efficacy of viral-mediated conditional knockout of MORs was assessed with brain slice electrophysiology on MOR-cKO mice, and compared to GFP mice, and uninjected $MOR^{fl/fl}$ controls. Mice were anesthetized with isoflurane and decapitated. The brain was removed, blocked and mounted in a vibratome chamber (Leica VT 1200S, Leica Biosystems, Buffalo Grove, IL, USA). Coronal slices (230 μm) containing the KF or preBötC (identified based on anatomical markers and coordinates from Franklin and Paxinos, 2008) were cut in ice-cold artificial cerebrospinal fluid (ACSF) that contained the following (in mM): 126 NaCl, 2.5 KCl, 1.2 MgCl2, 2.4 $CaCl_2$, 1.2 NaH_2PO_4, 11 D-glucose and 21.4 $NaHCO_3$ (equilibrated with 95% O_2/5% CO_2). Slices were stored at 32°C in glass vials with equilibrated ACSF. MK801 (10 μM) was added to the cutting solution and for the initial incubation of slices in storage (at least 30 min) to block NMDA receptor-mediated excitotoxicity. Following incubation, the slices were transferred to a recording chamber that was perfused with equilibrated ACSF warmed to 34°C (Warner Instruments) and flowing at a rate of 1.5–3 ml/min.

Cells were visualized using an upright microscope (Olympus BX51WI or Nikon FN1) equipped with custom built IR-Dodt gradient contrast illumination and DAGE-MTI IR-1000 camera. GFP fluorescence was identified in infected cells using LED epifluorescent illumination, GFP excitation/emission filter cube and detected using a DAGE-MTI IR-1000 camera with sufficient sensitivity in the GFP emission range.

Whole-cell recordings from KF neurons were performed with an Axopatch 200B amplifier (Molecular Devices, Sunnyvale, CA) in voltage-clamp (V_{hold}= −60mV) or current clamp mode. Whole-cell recordings from preBötC neurons were performed with a Multiclamp 700B amplifier (Molecular Devices, Sunnyvale, CA) in voltage-clamp (V_{hold}= −60mV) mode. Recording pipettes (1.5 – 3 MΩ) were filled with internal solution that contained (in mM): 115 potassium methanesulfonate, 20 NaCl, 1.5 $MgCl_2$, 5 HEPES(K), 2 BAPTA, 1–2 Mg-ATP, 0.2 Na-GTP, adjusted to pH 7.35 and 275–285 mOsM. Liquid junction potential (10 mV) was not corrected. Data were filtered at 10 kHz and collected at 20 kHz with AxographX or pClamp10.7, or collected at 400 Hz with PowerLab (Lab Chart version 5.4.2; AD Instruments, Colorado Springs, CO). I-V relationships were determined with a series of 10 mV voltage steps (−50 to −140 mV) at baseline and during perfusion of ME. The control I-V was subtracted from the I-V during ME to determine the reversal potential of the ME-mediated current. Series resistance was monitored without compensation and remained < 15

MΩ for inclusion. Drugs (including ME and baclofen) were applied by bath perfusion at the indicated concentrations. Bestatin (10 μM) and thiorphan (1 μM) were included with ME to prevent degradation.

Drugs

Morphine sulfate was obtained from the National Institute on Drug Abuse Drug Supply Program (RTI International, Research Triangle Park, NC). ME ([Met^5]-enkephalin acetate salt), bestatin HCl, DL-thiorphan and MK801 were from Sigma-Aldrich (St. Louis, MO). (RS)-baclofen was from Tocris (Minneapolis, MN).

Statistics

All statistical analyses were performed in GraphPad Prism 8. All error bars represent SEM unless otherwise stated. Data with $n > 8$ were tested for normality with Kolmogorov-Smirnov tests. For normally distributed data, comparisons between two groups were made using two-tailed *t*-tests. Comparisons between three or more groups were made using one-way ANOVA or two-way ANOVA followed by Tukey's post-hoc test or Holm-Sidak post hoc test.

Results

Conditional deletion of MORs from the KF and preBötC.

Mu-opioid receptors (MORs) are present throughout the majority of the lower brainstem (Mansour et al., 1994; Lonergan et al., 2003). Thus, opioids may influence a variety of respiratory neurons, such as those involved in the generation of the respiratory rhythm (preBötC neurons), or regulation of rate and stability of the rhythm (KF neurons). To directly compare the role of opioid-sensitive preBötC and KF neurons in opioid-induced respiratory depression, we used mice with floxed MORs (MOR$^{fl/fl}$) to conditionally delete MORs from these distinct brainstem respiratory groups (Weibel et al., 2013; Lutz et al., 2014).

GFP or Cre-GFP was virally expressed bilaterally in the KF of MOR$^{fl/fl}$ mice. Correct bilateral expression was confirmed in 33 of 47 mice by visualized GFP fluorescence (KF-GFP n = 13; KF MOR-cKO n = 20; Figure 1A and E). Based on immunohistochemistry against NeuN and GFP in a representative subset of mice (n = 3 mice), 65 % of neurons (range: 61–71%) in the injection site were infected and expressed GFP (Figure 1B).

In parallel experiments, GFP or Cre-GFP was similarly expressed in the preBötC of MOR$^{fl/fl}$ mice. Correct bilateral expression in the preBötC was confirmed in 36 out of 61 mice by visualizing GFP fluorescence (preBötC-GFP n = 17; preBötC MOR-cKO n = 19; Figure 1C and F). In a subset of mice (n = 5) we also verified that Cre-GFP expression was co-localized with somatostatin expression (a widely used marker for the preBötC [Stornetta et al., 2002; Cui et al., 2016]; Figure 1C and D). Based on immunohistochemistry against NeuN and GFP (n = 4 mice), 74% of neurons (range: 63–87%) in the injection site were infected and expressed GFP.

To provide functional evidence of MOR deletion, we performed whole-cell voltage-clamp recordings from KF and preBötC neurons in acute brain slices. Activation of somatodendritic MORs on a proportion (61%) of KF neurons causes an outward current that is mediated by G protein-coupled inwardly rectifying potassium (GIRK) conductance (Levitt *et al.*, 2015). In naïve or GFP-injected $MOR^{fl/fl}$ mice, the endogenous opioid agonist [Met^5]-enkephalin (ME; 1 μM) caused an outward current in 15 of 23 (65 %) KF neurons (Figure 2A). The GABA-B receptor agonist baclofen (30 μM) also caused an outward current in every opioid-sensitive KF neuron (mean amplitude = 38 ± 9 pA). The amplitude of the baclofen-mediated current correlated with the amplitude of the ME-induced current (r^2 = 0.76, Pearson's correlation, p = 0.001, n = 10). Therefore, the amplitude of the ME-mediated current was normalized to the baclofen-mediated current for comparisons between cells. In recordings from KF neurons from naïve or GFP-injected mice, ME (1 μM) caused an outward current that was 161 ± 14 % of baclofen (n = 4) or 153 ± 25 % of baclofen (n = 5), respectively (Figure 2B). Across all fluorescent neurons that we recorded from mice that were injected with Cre-GFP (Cre-GFP+), the ME-mediated current was abolished (−0.04 ± 2 % of baclofen, n = 11; Figure 2A and B), providing physiological confirmation of functional MOR removal from Cre-expressing KF neurons.

In current-clamp recordings, KF neurons were not typically spontaneously active, but would fire action potentials in response to current steps (50 – 250 pA, 2 s). In control mice (naïve/GFP-injected), the opioid/baclofen-sensitive KF neurons fired action potentials more slowly across the range of current steps (Figure 2C). The action potentials in opioid/baclofen-sensitive KF neurons had a broader half-width and smaller afterhyperpolarization (AHP) compared to non-sensitive neurons ([AP half-width: opioid-sensitive 1.34 ± 0.08 ms vs. non-sensitive 0.91 ± 0.09 ms, n = 15–18, p = 0.016 unpaired *t*-test], [AHP: opioid-sensitive 23.5 ± 1.7 mV vs. non-sensitive 32.7 ± 1.6 mV, n = 15–18, p = 0.0004 unpaired *t*-test]). These intrinsic properties that define the population of opioid-sensitive KF neurons are similar to previous results in KF neurons from rat (Levitt et al., 2015). In addition, input resistance was not different between opioid-sensitive (312 ± 43 MΩ, n = 14) and non-sensitive (424 ± 59 MΩ, n = 8) KF neurons (p = 0.14 unpaired *t*-test). Resting membrane potential was different between opioid-sensitive (−71 ± 2 mV, n = 14) and non-sensitive (−61 ± 1.5 mV, n = 8) KF neurons (p = 0.004 unpaired *t*-test). Importantly, deleting MORs had no effect on action potential firing (Figure 2C), action potential half-width (1.44 ± 0.22 ms, n = 7, p = 0.625 unpaired *t*-test), AHP (23.8 ± 3.5 mV, n = 7, p = 0.928 unpaired *t*-test), input resistance (333 ± 60 MΩ, n = 10, p = 0.777 unpaired *t*-test) or resting membrane potential (−67 ± 2.4 mV, n = 11, p = 0.21 unpaired *t*-test) in Cre-GFP+ baclofen-sensitive neurons. Thus, the intrinsic properties of opioid/baclofen-sensitive KF neurons were not altered by MOR deletion.

Similarly, we performed whole-cell voltage-clamp recordings from preBötC neurons in slices from naïve, GFP-injected and Cre-GFP injected $MOR^{fl/fl}$ adult mice. In slices from naïve $MOR^{fl/fl}$ mice (n = 5 mice), the opioid agonist ME (3 μM) caused an outward current in 4 out of 12 neurons (mean amplitude = 12 ± 2 pA; Figure 2D). In slices from GFP-injected mice (n = 3 mice), ME caused an outward current in 4 out of 15 GFP+ neurons (mean amplitude = 31 ± 7 pA). Since these currents were relatively small (consistent with previous reports (Lorier *et al.*, 2008)), we verified that they were GIRK-mediated using the current-voltage relationship. Responses that increased in conductance and reversed near E_K

were considered ME-mediated GIRK currents (Figure 2E; mean reversal potential of ME currents = −91 mV, n = 8). In slices from Cre-GFP mice (n = 4 mice), ME caused an outward current in 0 out of 13 neurons (Figure 2D), confirming deletion of functional MORs from Cre-expressing preBötC neurons. The intrinsic properties (capacitance and input resistance) of GFP and Cre-GFP expressing neurons were not different (Cm: GFP = 21 ± 3 pF, Cre-GFP = 17 ± 2 pF, p = 0.302 unpaired *t*-test; Rm: GFP = 554 ± 100 MΩ, Cre-GFP = 481 ± 63 MΩ, p = 0.556 unpaired t-test). Together, these results indicate that Cre-infected $MOR^{fl/fl}$ KF and preBötC neurons do not express functional MORs.

Differential contribution of KF and preBötC MORs to morphine-induced respiratory rate depression

To determine the effect of conditional deletion of MORs from KF and preBötC neurons on respiration in awake mice, we used plethysmography 4–5 weeks following injection of GFP or Cre-GFP expressing viruses. By challenging the animals with systemic morphine, we aimed to elucidate the specific functional contribution of KF and preBötC neurons to opioid-induced changes in respiration, specifically changes in average rate, pattern variability and apneas. A range of doses in semi-log increments (10, 30, 100 mg/kg) were chosen to reveal the effects of an anti-nociceptive dose (10 mg/kg), and of a safe, but near maximal respiratory rate depressant dose (100 mg/kg) (Dahan *et al.*, 2001; Romberg *et al.*, 2003; Weibel *et al.*, 2013; Kliewer *et al.*, 2019). The respiratory depressant effects of morphine (10–100 mg/kg) are due to activation of MORs, since they are eliminated in the global MOR knockout mice (Dahan *et al.*, 2001).

Mice were first injected with saline to establish a baseline respiratory rate for each trial. Baseline respiratory rates following saline administration were similar in all groups (KF-GFP, KF-MOR-cKO, preBötC-GFP and preBötC-MOR-cKO) when compared to naïve $MOR^{fl/fl}$ mice ($F(4,101) = 2.239$, $p = 0.0700$; individual comparisons to $MOR^{fl/fl}$ mice: KF-GFP $p = 0.1068$; KF MOR-cKO $p = 0.0505$; preBötC-GFP $p = 0.9537$; preBötC MOR-cKO $p = 0.0800$, by one-way ANOVA and Bonferroni post-hoc test, n = 19–28). Thus, even though global MOR knockout mice have increased baseline breathing frequency (Dahan et al., 2001), these results indicate a lack of endogenous MOR suppression of breathing following deletion of MORs from either the KF or preBötC alone.

Morphine-induced respiratory rate was normalized to the respective saline baseline respiratory rate within each trial, and is reported as the % of saline baseline rate. GFP expression alone in the KF or the preBötC did not change the magnitude of morphine-induced rate reduction when compared to naïve $MOR^{fl/fl}$ controls ($F(2,46) = 0.156$, $p = 0.856$; KF-GFP $p = 0.893$; preBötC-GFP $p = 0.997$, one-way ANOVA followed by Tukey's post-hoc test). Therefore, only comparisons between GFP and Cre-GFP groups are reported hereafter.

Morphine dose and conditional deletion of MORs from KF neurons had a significant overall effect on respiratory depression ($F(2,56) = 21.16$, $p < 0.0001$ and $F(2,56) = 21.90$, $p < 0.0001$, respectively; two-way ANOVA; Figure 3A). Respiratory rate reduction was significantly attenuated in KF MOR-cKO mice when compared to KF-GFP mice in response to all doses of morphine (Figure 3A; 10 mg/kg: $p = 0.0024$, 30 mg/kg: $p = 0.0171$, 100

mg/kg: p = 0.0002, two-way ANOVA followed by Tukey's post-hoc test). In mice with Cre injections that missed the KF (n = 7; including the lateral parabrachial area among others), morphine (10 mg/kg)-induced respiratory depression was similar to GFP control mice (53 ± 3 % of saline baseline, p = 0.3022; unpaired *t*-test). Thus, removal of MORs from the KF prevented a significant amount of morphine-induced rate reduction and retained a faster breathing rate even after high-dose morphine. These results suggest that high-doses of opioids cause severe respiratory depression partially due to direct effects on KF neurons.

Similar to the KF experiments described above, morphine dose and conditional removal of MORs from the preBötC also had a significant overall impact on respiratory rate reduction ($F(2,57) = 60.45$, $p < 0.0001$ and $F(2,57) = 7.476$, $p = 0.0013$, respectively; two-way ANOVA; Figure 3B). However, respiratory rate reduction was only significantly attenuated in preBötC MOR-cKO mice compared to preBötC-GFP controls when challenged with the low dose of morphine (10 mg/kg: $p < 0.0001$, two-way ANOVA followed by Tukey's post-hoc test; Figure 3B). Surprisingly, conditional deletion of MORs from the preBötC did not have a significant effect on respiratory depression following administration of higher doses of morphine (30 mg/kg: p = 0.4187; 100 mg/kg: p = 0.5389; two-way ANOVA followed by Tukey's post-hoc test).

In direct comparison of the KF MOR-cKO and preBötC MOR-cKO groups, there was a similar reduction in respiratory rate after administration of the lowest dose of morphine (Figure 3C; KF MOR-cKO vs. preBötC MOR-cKO - 10 mg/kg: p = 0.4224 unpaired *t*-tests). However, the medium and highest doses of morphine reduced rate significantly less in the KF MOR-cKO mice (30 mg/kg: p = 0.0212; 100 mg/kg: p = 0.0047, unpaired *t*-test; Figure 3C). These results indicate that both KF and preBötC MORs contribute to changes in breathing frequency when challenged with a therapeutically relevant, low-dose of morphine. However, higher doses of opioids may further depress respiratory rate by inhibiting other respiratory brainstem nuclei, including, but not limited to, the KF.

MOR-deletion from preBötC neurons shortens inspiration

Decreases in respiratory rate can be the result of a proportionate increase in the duration of inspiration (T_i) and expiration (T_e) equally, or a disproportionate increase in either. Since reductions in respiratory rate by low-dose morphine (10 mg/kg) were attenuated in both KF and preBötC MOR-cKO mice and the respiratory traces following low-dose morphine administration did not contain any visible ataxic patterns, we used these experiments to decipher the changes in respiratory phases that led to the depression of rate (Figure 4). The average T_i and T_e were analyzed in representative segments of respiratory traces from MOR-cKO and GFP injected animals (see example in Figure 4A).

As expected, morphine exposure led to a significant increase in both average T_i and average T_e compared to the saline baseline in every group, thus causing the slowing of rate (GFP and MOR-cKO groups separately, saline vs. morphine; $p < 0.05$ with paired *t*-test, Figure 4B and C). These data demonstrate that systemic administration of morphine slows breathing by increasing both inspiration and expiration.

To determine the effect of MOR knockout in each area, we compared the mice with Cre-GFP to control mice with GFP expression in the same area. Conditional knockout of MORs from the KF did not significantly change morphine-induced T_i or T_e (T_i: $p = 0.408$; T_e: $p = 0.212$; unpaired *t*-test; Figure 4B). Therefore, removal of KF MORs did not cause disproportionate changes in the respiratory phases, but an overall, proportionate rate effect. This result supports the role of the KF as a respiratory rate modulator.

Conditional deletion of MORs from the preBötC resulted in significantly shorter morphine-induced T_i ($p = 0.011$; unpaired *t*-test), but did not affect the duration of T_e ($p = 0.707$; unpaired *t*-test; Figure 4C). Thus, the faster respiratory rate of preBötC MOR-cKO mice after low-dose morphine is due to the shortening of inspiration, which leads to more frequent inhalations and an increased rate. This aligns with the role of the preBötC as the inspiratory rhythm generator, and suggests that the lengthening of the inspiratory phase caused by low dose opioids is mainly caused by the inhibition of inspiratory preBötC neurons.

Ataxic breathing following administration of high-dose morphine

Opioids not only depress respiratory rate, but also cause irregular breathing patterns (ataxic breathing) that often contain apneas, defined by long pauses between breaths (Bouillon *et al.*, 2003). In rats and mice, both rate depression and changes in pattern have been directly linked to the inspiratory output from the preBötC rhythm generating network (Mellen *et al.*, 2003; McKay *et al.*, 2005; Pattinson, 2008). Additionally, the KF can influence rate variability by modulating the activity of the preBötC, a function that may be less efficient or potentially lost under the influence of opioids (Jiang *et al.*, 2004; Rybak *et al.*, 2004; Dutschmann & Dick, 2012; Dhingra *et al.*, 2017).

We found that administration of high doses of morphine (30 and 100 mg/kg) leads to ataxic respiratory patterns, demonstrating intermixed fast and slow respiratory rates in all groups. There were especially noticeable differences in the pattern of breathing between KF and preBötC conditional knockout groups in response to the highest morphine dose (100 mg/kg dose, Figure 5). KF-MOR-cKO mice and GFP controls had variable rates of breathing, but smooth inspiration and expiration phase transitions (Figure 5A1, A2 and B1). In contrast, the slow breathing periods in preBötC-MOR-cKO mice consisted of shallow expiratory periods followed by triangular inspiratory efforts, which resembled gasping (Figure 5B2, gasping pattern highlighted in gray). The substantial increase in pattern irregularity caused by the highest dose of morphine when compared to saline is also demonstrated by the increased cycle-to-cycle spread in T_{Tot} in the Poincaré plots shown in Figure 6. Noticeably, the representative example Poincaré plot for the KF MOR-cKO group indicates less variability under the influence of high dose morphine compared to the other groups (Figure 6B vs. A, C and D).

To quantify the amount of variability in the breathing pattern illustrated by the example traces and Poincaré plots, we next performed a coefficient of variation (CV%) analysis of the instantaneous respiratory frequency of each subject during the steady-state of saline and morphine trials. The results of coefficient of variation (CV%) analysis in Figure 6 further support a morphine-induced dose-dependent increase in respiratory pattern variability ($F(11,170) = 11.80$, $p < 0.0001$ two-way ANOVA). The CV% analysis did not show

increased amounts of variability in any group following 10 mg/kg morphine compared to saline baseline. However, 30 mg/kg morphine resulted in a significant increase in CV% in every group. This effect did not increase in severity following the highest 100 mg/kg dose, indicating that the maximal effect on the breathing pattern variability is reached by 30 mg/kg morphine (Figure 6). Additionally, the amount of variability indicated by the CV% was statistically similar between treatment groups (GFP vs. MOR-cKO groups, as well as KF MOR-cKO vs. preBötC MOR-cKO) at all doses ($p > 0.05$ by two-way ANOVA followed by Holm-Sidak post-hoc test, Figure 6. CV% summary bar graphs). These results suggest that, while morphine-induced ataxic pattern characteristics may differentially depend on KF and/or preBötC MOR-activation, the level of rate variability does not.

In addition to rate variability, a major contributing factor to respiratory ataxia is the occurrence of apneas following morphine administration (see example trace in Figure 7A). Morphine dose-dependently increased the number of apneas occurring in the 45 minutes following morphine injection ($F(2,83) = 8.036$, $p = 0.0006$; two-way ANOVA; Figure 7B). The location of conditional MOR deletion also significantly affected apnea counts ($F(3,83) = 11.13$, $p < 0.0001$; two-way ANOVA followed by Tukey's post-hoc test; Figure 7B). At the 30 mg/kg dose the preBötC MOR-cKO group displayed significantly more apneas than any other group (preBötC MOR-cKO vs. KF-MOR-cKO $p < 0.0001$, preBötC MOR-cKO vs. preBötC-GFP $p < 0.0001$, preBötC MOR-cKO vs. KF-GFP $p = 0.0004$; Figure 7B). Thus, surprisingly deletion of MORs in the preBötC increases the appearance of apneas. In contrast, the KF MOR-cKO group had a very low number of apneas.

Discussion

Understanding the mechanisms whereby opioids modulate respiratory neurons is valuable, not only because of the clinical and economic impact of overdoses, but also to gain insight into the basic function of opioid-sensitive respiratory networks. Here, we investigated the specific role of MORs in KF and preBötC neurons in opioid-induced respiratory depression in awake adult mice using a conditional genetic knockout approach. The results revealed dose-dependent region-specific opioid effects on the control of both respiratory rate and pattern. Knockout of MORs in KF neurons attenuated morphine-induced rate suppression at all doses. Deletion of MORs in the preBötC attenuated morphine-induced rate suppression at the anti-nociceptive dose, but surprisingly had no effect on rate following high doses of morphine. Instead, a severe ataxic breathing pattern emerged with increased variability and many apneas. These results suggest that countering opioid effects in the KF, which provides excitatory respiratory drive to many of the medullary respiratory centers (Song *et al.*, 2012; Yokota *et al.*, 2015; Geerling *et al.*, 2017; Molkov *et al.*, 2017), may be an attractive approach to combat opioid overdose. We conclude that opioids affect distributed areas of the respiratory network and opioid-induced respiratory depression cannot be attributed to only one area in isolation.

Comparison to pharmacological studies on the role of KF and preBötC in opioid-induced rate suppression

The majority of previous studies on the respiratory rate depressant effects of opioids have used locally applied opioid agonists and antagonists into the KF or preBötC to induce or prevent/reverse opioid effects on rate, and have yielded conflicting results regarding the major site of opioid-induced respiratory depression in the brainstem (Lalley, 2003; Mustapic *et al.*, 2010; Montandon *et al.*, 2011, 2016; Prkic *et al.*, 2012; Lalley *et al.*, 2014; Montandon & Horner, 2014; Stucke *et al.*, 2015; Levitt *et al.*, 2015; Miller *et al.*, 2017). One concern and a potential source of conflicting experimental outcomes is that it is unknown if the above described effects were due to activation of somatodendritic or presynaptic receptors in the local area, with one exception (Montandon *et al.*, 2016). Additionally, a locally applied antagonist leaves receptors on terminals in projection regions unblocked. Thus, even though neuronal firing will be restored for neurons in the local area, release from terminals in projection areas will remain inhibited by systemic opioid administration. The net physiological result for projection neurons will still be inhibition. There are dense reciprocal projections between the KF and the preBötC, thus projection neurons likely play an important role in the activity of neurons in these regions (Ezure & Tanaka, 2006; Tan *et al.*, 2010; Song *et al.*, 2012; Yokota *et al.*, 2015; Geerling *et al.*, 2017; Yang & Feldman, 2018).

We used a genetic approach to delete MORs from both the somatodendritic local area and from terminals in projection regions to provide insights into the role of KF and preBötC neurons in opioid-induced respiratory disturbances. In our experiments, presynaptic MORs on projections into the local area remained intact, whereas these receptors would be inhibited by local antagonist. Our results indicate that MOR-containing KF neurons and preBötC neurons (including projection neurons) equally contribute to respiratory depression caused by an anti-nociceptive dose of morphine (10 mg/kg), since deletion of MORs from these regions resulted in similarly attenuated morphine effects. However, respiratory rate depression was not eliminated in either the KF MOR-cKO or the preBötC MOR-cKO group indicating a distributed, network-wide effect of opioids at therapeutically relevant doses. This interpretation is supported by findings that the KF and preBötC both partially contribute to respiratory depression induced by clinically relevant doses of remifentanil (Stucke *et al.*, 2015; Miller *et al.*, 2017). An alternative explanation is that remaining MORs in either region from partial knockout are sufficient to induce the residual respiratory depression.

We then increased the morphine dose to induce close to maximum respiratory depressant effects. These experiments demonstrated a differential influence of morphine on KF and preBötC neurons resulting in site-specific respiratory changes. Deletion of MORs in the KF, but not the preBötC, significantly attenuated morphine-induced suppression of rate. This result indicates that the loss of excitatory respiratory drive provided by the KF contributes to opioid-induced respiratory rate suppression at high doses of morphine.

Ataxic breathing following high-dose morphine was exaggerated in preBötC MOR-cKO

Opioids not only depress respiratory rate, but at high doses, cause irregular breathing patterns with increasing amounts of apneas and decreased tidal volume. Such effects on tidal

volume and pattern have been observed in humans acutely treated with alfentanil and correlated with the severity of rate depression (Bouillon *et al.*, 2003). While our methods were not optimal for accurate tidal volume measurements, we were able to analyze morphine-induced changes in pattern variability. Animal studies linked opioid-induced respiratory pattern transformation to changes in motor output due to 'quantal slowing' of preBötC bursting, wherein increased expiratory periods result from skipped inspirations in the preBötC (Mellen *et al.*, 2003; Pattinson, 2008; Lal *et al.*, 2011; Baesens & MacKay, 2013). We did not observe quantal slowing in any experimental group, which could be due to multiple variables. In the study by Mellen and colleagues (2003), quantal slowing was more apparent in anesthetized, vagotomized juvenile rats in response to fentanyl, while we used morphine in adult, awake, vagi-intact mice. However, high doses of morphine did significantly increase the variability in breathing rate in all groups, which occurred as stereotypical, intermittent clusters of fast and slow breaths. These patterns are comparable to the sleep-disordered breathing patterns observed following ablation of the preBötC (McKay *et al.*, 2005; McKay & Feldman, 2008) and in chronic opioid users who also display sleep apnea (Farney *et al.*, 2008, 2013). Thus, considering the sedative effects of opioids, it is not unlikely that the patterns observed in our experiments include periods of sleep interrupted by periods of arousal with increased respiratory drive to compensate for the potentially hypoxic/hypercapnic state of the animal. The neural basis and physiologic effects of arousal on respiratory drive during opioid overdose should be addressed in detail by future studies.

Interestingly, we found that high doses of morphine caused significantly more apneas in the breathing pattern of preBötC MOR-cKO animals. This is counterintuitive since preBötC neurons should be more excitable and thus reach threshold potentials more easily in preBötC MOR-cKO mice. A possible explanation for these results is that hyperexcitability of inspiratory preBötC neurons led to a "refractory period" unable to generate inspiratory bursts (Baertsch *et al.*, 2018). It is becoming increasingly evident that inhibition plays an important role in respiratory frequency (Cregg *et al.*, 2017; Baertsch *et al.*, 2018; Ramirez & Baertsch, 2018). Local inhibition during inspiratory bursts prevents hyperactivity and accompanying long refractory periods resulting in higher inspiratory rates. Additionally, the effects of local inhibition can be further facilitated by vagal sensory feedback originating from the lung stretch receptors that project to preBötC and KF, among other areas (Dhingra *et al.*, 2017; Baertsch *et al.*, 2018). Inspiratory bursting, predominately excitatory, neurokinin-1 receptor (NK1R)-expressing preBötC neurons are highly opioid-sensitive (Gray *et al.*, 1999; Montandon *et al.*, 2011). Removing MORs from these excitatory, inspiratory preBötC neurons would prevent opioid inhibition and make them more excitable than the rest of the respiratory network. At the same time, the systemically administered opioids would also inhibit the vagal sensory feedback loop (Poole *et al.*, 2007), and additional opioid-sensitive modulatory inputs. Therefore, inspiratory, excitatory preBötC neurons may be relatively hyperexcited compared to the rest of the network due to reduced inhibition, which would lead to slower respiratory rates and highly irregular respiratory patterns, as well as apneas due to the skipped inspiratory cycles. Our approach led to non-selective expression of Cre in all neurons in the infected area, which did not allow us to test the role of specific subpopulations of opioid-sensitive excitatory/inhibitory neurons in this region. Since ablation of all NK1R+ preBötC neurons leads to ataxia (McKay *et al.*, 2005),

future studies using targeted MOR deletion from NK1R+ neurons are needed to directly address this hypothesis.

In contrast, depletion of MORs from the KF resulted in higher respiratory rate and less apneic events in the breathing patterns. The KF provides excitatory respiratory drive to the majority of the medullary respiratory centers, including the preBötC (Song *et al.*, 2012; Yokota *et al.*, 2015; Geerling *et al.*, 2017). Following the above hypothesis, in the KF MOR-cKO mice, the KF neurons are not inhibited by morphine and appear to provide enough regulatory input to the preBötC and other respiratory centers to somewhat stabilize the rate and patterning of the respiratory motor output. Supporting evidence from other studies indicates that the KF plays a role in regulating the rate and stability of the respiratory rhythm (Dutschmann & Herbert, 2006; Pattinson, 2008; Guyenet & Bayliss, 2015; Cregg *et al.*, 2017; Dhingra *et al.*, 2017).

Contribution of nearby areas

An advantage of our approach is that we are able to visualize the spread of infected cells to minimize including animals with unintended targeted areas. Nevertheless, low levels of Cre expression could occur in nearby/adjacent neighboring areas. For instance, the KF is in close proximity to the lateral parabrachial nucleus, a respiratory region implicated in mediating arousal, hence increased breathing frequency, induced by hypercapnia (Chamberlin, 2013; Kaur *et al.*, 2013; Palmiter, 2018). While it is unknown if arousal-mediating parabrachial neurons express MORs, infection of such neurons could potentially contribute to the attenuated respiratory rate depression. However, animals with missed injections infecting regions outside of the KF (often including the parabrachial complex) showed similar levels of respiratory depression to the GFP and uninjected control groups. Arousal-promoting projections also exist from the preBötC to locus coeruleus (Yackle *et al.*, 2017). It is unknown if these neurons contain MORs and if they could contribute to opioid-induced respiratory depression.

In summary, using selective genetic ablation of MORs from distinct populations of respiratory neurons in the medulla and pons, this study shows that opioid-induced respiratory depression, similar to opioid-induced analgesia, is the result of distributed network effects caused at multiple sites of action. Future studies determining the molecular identities of the neurons involved, as well as their functional connections in the respiratory network, will be crucial to advance the understanding of opioid regulation of the respiratory circuitry.

Acknowledgements:

We thank Drs. John Bissonnette, Dan Wesson and Brooks Robinson for helpful comments and feedback on the manuscript.

Funding: This work was supported by National Institutes of Health Grants DA038069 (E.S.L.) and DA05010 (B.L.K.). A.G.V. was funded by the UF Breathing Research and Therapeutics Training Program (T32 HL134621) and the Center for Respiratory Research and Rehabilitation.

References

Baertsch NA, Baertsch HC & Ramirez JM (2018). The interdependence of excitation and inhibition for the control of dynamic breathing rhythms. Nat Commun 9, 1–17. [PubMed: 29317637]

Baesens C & MacKay RS (2013). Analysis of a scenario for chaotic quantal slowing down of inspiration. J Math Neurosci 3, 1–17. [PubMed: 23343328]

Bouillon T, Bruhn J, Roepcke H & Hoeft A (2003). Opioid-induced respiratory depression is associated with increased tidal volume variability. Eur J Anaesthesiol 20, 127–133. [PubMed: 12622497]

Chamberlin NL (2013). Brain circuitry mediating arousal from obstructive sleep apnea. Curr Opin Neurobiol 23, 774–779. [PubMed: 23810448]

Cregg JM, Chu KA, Dick TE, Landmesser LT & Silver J (2017). Phasic inhibition as a mechanism for generation of rapid respiratory rhythms. Proc Natl Acad Sci 114, 12815–12820. [PubMed: 29133427]

Cui Y, Kam K, Sherman D, Janczewski WA, Zheng Y & Feldman JL (2016). Defining preBötzinger Complex Rhythm- and Pattern-Generating Neural Microcircuits In Vivo. Neuron 91, 602–614. [PubMed: 27497222]

Dahan A, Aarts L & Smith TW (2010). Incidence, reversal, and prevention of opioid-induced respiratory depression. Anesthesiology 112, 226–238. [PubMed: 20010421]

Dahan A, Sarton E, Teppema L, Olievier C, Nieuwenhuijs D, Matthes HWD & Kieffer BL (2001). Anesthetic potency and influence of morphine and sevoflurane on respiration in μ-opioid receptor knockout mice. Anesthesiology 94, 824–832. [PubMed: 11388534]

Dhingra RR, Dutschmann M, Galán RF & Dick TE (2017). Kölliker-Fuse nuclei regulate respiratory rhythm variability via a gain-control mechanism. Am J Physiol - Regul Integr Comp Physiol 312, R172–R188. [PubMed: 27974314]

Dutschmann M & Dick TE (2012). Pontine mechanisms of respiratory control. Compr Physiol 2, 2443–2469. [PubMed: 23720253]

Dutschmann M & Herbert H (2006). The Kölliker-Fuse nucleus gates the postinspiratory phase of the respiratory cycle to control inspiratory off-switch and upper airway resistance in rat. Eur J Neurosci 24, 1071–1084. [PubMed: 16930433]

Ezure K & Tanaka I (2006). Distribution and medullary projection of respiratory neurons in the dorsolateral pons of the rat. Neuroscience 141, 1011–1023. [PubMed: 16725272]

Farney RJ, McDonald AM, Boyle KM, Snow GL, Nuttall RT, Coudreaut MF, Wander TJ & Walker JM (2013). Sleep disordered breathing in patients receiving therapy with buprenorphine/naloxone. Eur Respir J 42, 394–403. [PubMed: 23100497]

Farney RJ, Walker JM, Boyle KM, Cloward TV. & Shilling KC (2008). Adaptive servoventilation (ASV) in patients with sleep disordered breathing associated with chronic opioid medications for non-malignant pain. J Clin Sleep Med 4, 311–319. [PubMed: 18763421]

Feldman JL, Mitchell GS & Nattie EE (2003). Breathing: rhythmicity, plasticity, chemosensitivity. Annu Rev Neurosci 26, 239–266. [PubMed: 12598679]

Franklin KBJ & Paxinos G (2008). The mouse brain in stereotaxic coordinates, Third edit.ed. Menzel J. Academic Press, Elsevier, New York, NY.

Geerling JC, Yokota S, Rukhadze I, Roe D & Chamberlin NL (2017). Kölliker–Fuse GABAergic and glutamatergic neurons project to distinct targets. J Comp Neurol 525, 1844–1860. [PubMed: 28032634]

Gray PA, Rekling JC, Bocchiaro CM & Feldman JL (1999). Modulation of respiratory frequency by peptidergic input to rhythmogenic neurons in the preBotzinger complex. Science (80-) 286, 1566–1568. [PubMed: 10567264]

Grundy D (2015). Principles and standards for reporting animal experiments in The Journal of Physiology and Experimental Physiology. J Physiol 593, 2547–2549. [PubMed: 26095019]

Guyenet PG & Bayliss DA (2015). Neural Control of Breathing and CO2 Homeostasis. Neuron 87, 946–961. [PubMed: 26335642]

Hurlé MA, Mediavilla A & Flórez J (1985). Differential respiratory patterns induced by opioids applied to the ventral medullary and dorsal pontine surfaces of cats. Neuropharmacology 24, 597–606. [PubMed: 3927184]

Janczewski WA & Feldman JL (2006). Distinct rhythm generators for inspiration and expiration in the juvenile rat. J Physiol 570, 407–420. [PubMed: 16293645]

Jiang M, Alheid GF, Calandriello T & McCrimmon DR (2004). Parabrachial-lateral pontine neurons link nociception and breathing. Respir Physiol Neurobiol 143, 215–233. [PubMed: 15519557]

Kaur S, Pedersen NP, Yokota S, Hur EE, Fuller PM, Lazarus M, Chamberlin NL & Saper CB (2013). Glutamatergic signaling from the parabrachial nucleus plays a critical role in hypercapnic arousal. J Neurosci 33, 7627–7640. [PubMed: 23637157]

Kliewer A, Schmiedel F, Sianati S, Bailey A, Bateman JT, Levitt ES, Williams JT, Christie MJ & Schulz S (2019). Phosphorylation-deficient G-protein-biased μ-opioid receptors improve analgesia and diminish tolerance but worsen opioid side effects. Nat Commun 10, 367. [PubMed: 30664663]

Lal A, Oku Y, Hülsmann S, Okada Y, Miwakeichi F, Kawai S, Tamura Y & Ishiguro M (2011). Dual oscillator model of the respiratory neuronal network generating quantal slowing of respiratory rhythm. J Comput Neurosci 30, 225–240. [PubMed: 20544264]

Lalley PM (2003). μ-Opioid receptor agonist effects on medullary respiratory neurons in the cat: evidence for involvement in certain types of ventilatory disturbances. Am J Physiol - Regul Integr Comp Physiol 285, R1287–R1304. [PubMed: 12881202]

Lalley PM, Pilowsky PM, Forster HV. & Zuperku EJ (2014). CrossTalk opposing view: The pre-Bötzinger complex is not essential for respiratory depression following systemic administration of opioid analgesics. J Physiol 592, 1163–1166. [PubMed: 24634012]

Levitt ES, Abdala AP, Paton JFR, Bissonnette JM & Williams JT (2015). μ opioid receptor activation hyperpolarizes respiratory-controlling Kölliker-Fuse neurons and suppresses post-inspiratory drive. J Physiol 593, 4453–4469. [PubMed: 26175072]

Levitt ES, Hunnicutt BJ, Knopp SJ, Williams JT & Bissonnette JM (2013). A selective 5-HT1A receptor agonist improves respiration in a mouse model of Rett syndrome. J Appl Physiol 115, 1626–1633. [PubMed: 24092697]

Lonergan T, Goodchild AK, Christie MJ & Pilowsky PM (2003). Mu opioid receptors in rat ventral medulla: effects of endomorphin-1 on phrenic nerve activity. Respir Physiol Neurobiol 138, 165–178. [PubMed: 14609508]

Lorier AR, Lipski J, Housley GD, Greer JJ & Funk GD (2008). ATP sensitivity of preBötzinger complex neurones in neonatal rat in vitro: Mechanism underlying a P2 receptor-mediated increase in inspiratory frequency. J Physiol 586, 1429–1446. [PubMed: 18174215]

Mansour A, Fox CA, Burke S, Meng F, Thompson RC, Akil H & Watson SJ (1994). Mu, delta, and kappa opioid receptor mRNA expression in the rat CNS: an in situ hybridization study. J Comp Neurol 350, 412–438. [PubMed: 7884049]

McKay LC & Feldman JL (2008). Unilateral Ablation of Pre-Bötzinger Complex Disrupts Breathing during Sleep but Not Wakefulness. Am J Respir Crit Care Med 178, 89–95. [PubMed: 18420958]

McKay LC, Janczewski WA & Feldman JL (2005). Sleep-disordered breathing after targeted ablation of preBötzinger complex neurons. Nat Neurosci 8, 1142–1144. [PubMed: 16116455]

Mellen NM, Janczewski WA, Bocchiaro CM & Feldman JL (2003). Opioid-induced quantal slowing reveals dual networks for respiratory rhythm generation. Neuron 37, 821–826. [PubMed: 12628172]

Miller JR, Zuperku EJ, Stuth EAE, Banerjee A, Hopp FA & Stucke AG (2017). A Subregion of the Parabrachial Nucleus Partially Mediates Respiratory Rate Depression from Intravenous Remifentanil in Young and Adult Rabbits. Anesthesiology 127, 502–514. [PubMed: 28590302]

Molkov YI, Rubin JE, Rybak IA & Smith JC (2017). Computational models of the neural control of breathing. Wiley Interdiscip Rev Syst Biol Med; DOI: 10.1002/wsbm.1371.

Montandon G & Horner R (2014). The preBotzinger complex is essential for the respiratory depression following systemic administration of opioid analgesics. J Physiol 5926, 1159–1162.

Montandon G, Liu H & Horner RL (2016). Contribution of the respiratory network to rhythm and motor output revealed by modulation of GIRK channels, somatostatin and neurokinin-1 receptors. Sci Rep; DOI: 10.1038/srep32707.

Montandon G, Qin W, Liu H, Ren J, Greer JJ & Horner RL (2011). PreBotzinger Complex Neurokinin-1 Receptor-Expressing Neurons Mediate Opioid-Induced Respiratory Depression. J Neurosci 31, 1292–1301. [PubMed: 21273414]

Mortola JP & Noworaj A (1983). Two-sidearm tracheal cannula for respiratory airflow measurements in small animals. J Appl Physiol 55, 250–253. [PubMed: 6885578]

Mustapic S, Radocaj T, Sanchez A, Dogas Z, Stucke AG, Hopp F a, Stuth E a E & Zuperku EJ (2010). Clinically relevant infusion rates of mu-opioid agonist remifentanil cause bradypnea in decerebrate dogs but not via direct effects in the pre-Bötzinger complex region. J Neurophysiol 103, 409–418. [PubMed: 19906886]

Palmiter RD (2018). The Parabrachial Nucleus: CGRP Neurons Function as a General Alarm. Trends Neurosci 41, 280–293. [PubMed: 29703377]

Pattinson KTS (2008). Opioids and the control of respiration. Br J Anaesth 100, 747–758. [PubMed: 18456641]

Paxinos G & Franklin KBJ (2008). The mouse brain in stereotaxic coordinates - Third Edition. Acad Press1–350.

Poole SL, Deuchars J, Lewis DI & Deuchars SA (2007). Subdivision-Specific Responses of Neurons in the Nucleus of the Tractus Solitarius to Activation of Mu-Opioid Receptors in the Rat. J Neurophysiol 98, 3060–3071. [PubMed: 17898143]

Prkic I, Mustapic S, Radocaj T, Stucke AG, Stuth EAE, Hopp FA, Dean C & Zuperku EJ (2012). Pontine -opioid receptors mediate bradypnea caused by intravenous remifentanil infusions at clinically relevant concentrations in dogs. J Neurophysiol 108, 2430–2441. [PubMed: 22875901]

Ramirez J-M & Baertsch N (2018). Defining the Rhythmogenic Elements of Mammalian Breathing. Physiology 33, 302–316. [PubMed: 30109823]

Romberg R, Sarton E, Teppema L, Matthes HWD, Kieffer BL & Dahan A (2003). Comparison of morphine-6-glucuronide and morphine on respiratory depressant and antinociceptive responses in wild type and μ-opioid receptor deficient mice. Br J Anaesth 91, 862–870. [PubMed: 14633759]

Rudd RA, Seth P, David F & Scholl L (2016). Increases in Drug and Opioid-Involved Overdose Deaths — United States, 2010–2015. MMWR Morb Mortal Wkly Rep 65, 1445–1452. [PubMed: 28033313]

Rybak IA, Shevtsova NA, Paton JFR, Dick TE, St.-John WM, Mörschel M & Dutschmann M (2004). Modeling the ponto-medullary respiratory network. Respir Physiol Neurobiol 143, 307–319. [PubMed: 15519563]

Schindelin J, Arganda-Carreras I, Frise E, Kaynig V, Longair M, Pietzsch T, Preibisch S, Rueden C, Saalfeld S, Schmid B, Tinevez J-Y, White DJ, Hartenstein V, Eliceiri K, Tomancak P & Cardona A (2012). Fiji: an open-source platform for biological-image analysis. Nat Methods 9, 676. [PubMed: 22743772]

Song G, Wang H, Xu H & Poon CS (2012). Kölliker-Fuse neurons send collateral projections to multiple hypoxia-activated and nonactivated structures in rat brainstem and spinal cord. Brain Struct Funct 217, 835–858. [PubMed: 22286911]

John WM St. & Paton JFR (2004). Role of pontile mechanisms in the neurogenesis of eupnea. Respir Physiol Neurobiol 143, 321–332. [PubMed: 15519564]

Stornetta RL, Rosin DL, Wang H, Sevigny CP, Weston MC & Guyenet PG (2002). A group of glutamatergic interneurons expressing high levels of both neurokinin-1 receptors and somatostatin identifies the region of the pre-Bötzinger complex. J Comp Neurol 455, 499–512.

Stucke AG, Miller JR, Prkic I, Zuperku EJ, Hopp FA & Stuth EAE (2015). Opioid-induced Respiratory Depression Is only Partially Mediated by the preBötzinger Complex in Young and Adult Rabbits in Vivo. In Anesthesiology, pp. 1288–1298. [PubMed: 25751234]

Tan W, Pagliardini S, Yang P, Janczewski WA & Feldman JL (2010). Projections of prebötzinger complex neurons in adult rats. J Comp Neurol 518, 1862–1878. [PubMed: 20235095]

Volkow ND & Collins FS (2017). The Role of Science in Addressing the Opioid Crisis. N Engl J Med 377, 391–394. [PubMed: 28564549]

Weibel R, Reiss D, Karchewski L, Gardon O, Matifas A, Filliol D, Becker JAJ, Wood JN, Kieffer BL & Gaveriaux-Ruff C (2013). Mu Opioid Receptors on Primary Afferent Nav1.8 Neurons

Contribute to Opiate-Induced Analgesia: Insight from Conditional Knockout Mice. PLoS One 8, 1–18.

Wittmeier S, Song G, Duffin J & Poon C-S (2008). Pacemakers handshake synchronization mechanism of mammalian respiratory rhythmogenesis. Proc Natl Acad Sci 105, 18000–18005. [PubMed: 19008356]

Yackle K, Schwarz LA, Kam K, Sorokin JM, Huguenard JR, Feldman JL, Luo L & Krasnow MA (2017). Breathing control center neurons that promote arousal in mice. Science (80-) 355, 1411–1415. [PubMed: 28360327]

Yaksh T, Woller S, Ramachandran R & Sorkin L (2015). The search for novel analgesics: targets and mechanisms. F1000Prime Rep; DOI: 10.12703/P7-56.

Yaksh TL (1997). Pharmacology and mechanisms of opioid analgesic activity. Acta Anaesthesiol Scand 41, 94–111. [PubMed: 9061092]

Yang CF & Feldman JL (2018). Efferent projections of excitatory and inhibitory preBötzinger Complex neurons. J Comp Neurol 526, 1389–1402. [PubMed: 29473167]

Yokota S, Kaur S, Vanderhorst VG, Saper CB & Chamberlin NL (2015). Respiratory-related outputs of glutamatergic, hypercapnia-responsive parabrachial neurons in mice. J Comp Neurol 523, 907–920. [PubMed: 25424719]

Key points

- The main cause of death from opioid overdose is respiratory depression due to the activation of mu opioid receptors (MORs).
- We conditionally deleted MORs from neurons in two key areas of the brainstem respiratory circuitry (the Kölliker-Fuse nucleus (KF) or pre-Bötzinger complex (preBötC)) to determine their role in opioid-induced respiratory disturbances in adult, awake mice.
- Deletion of MORs from KF neurons attenuated respiratory rate depression at all doses of morphine.
- Deletion of MORs from preBötC neurons attenuated rate depression at the low dose, but had no effect on rate following high doses of morphine. Instead, high doses of morphine increased the occurrence of apneas.
- The results indicate that opioids affect distributed key areas of the respiratory network in a dose-dependent manner and countering the respiratory effects of high dose opioids via the KF may be an effective approach to combat overdose.

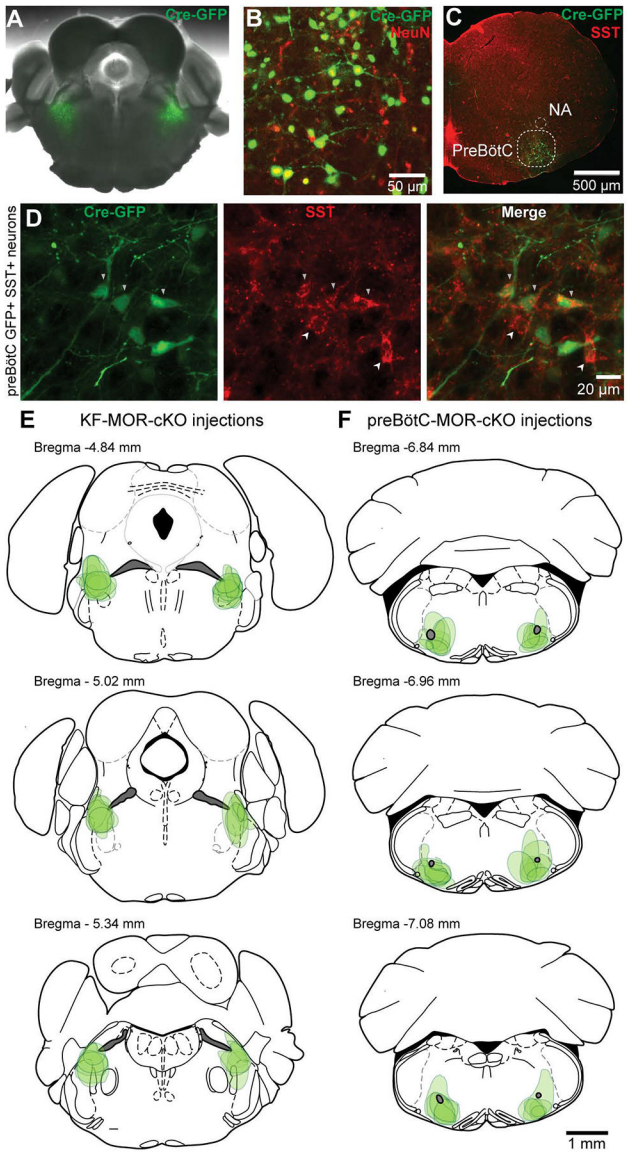

Figure 1. Identification of injection sites by immunohistochemistry.

A, Example AAV2-CMV-Cre-GFP injection (green) in the KF of a $MOR^{fl/fl}$ mice. **B**, Example of immunohistochemistry against NeuN and GFP to quantify viral expression in KF neurons. **C, D**, A representative example of a preBötC injection site. Correct placement of viral injections into the preBötC was verified based on anatomical landmarks (C) and somatostatin immunostaining (D). Nucleus ambiguus (NA). Arrowheads pointing down indicate GFP-SST co-expression, arrowheads pointing up indicate SST-expression only. **E, F** Estimated dorsal-ventral and medial-lateral borders of bilateral AAV2-CMV-Cre-GFP injection sites in the KF (E) and preBötC (F) based on visualized GFP fluorescence spread. Each green shaded shape represents a single injection site placed in the rostro-caudal plane where GFP expression was maximal. Schematics of mouse brain slices were created based upon (Paxinos & Franklin, 2008).

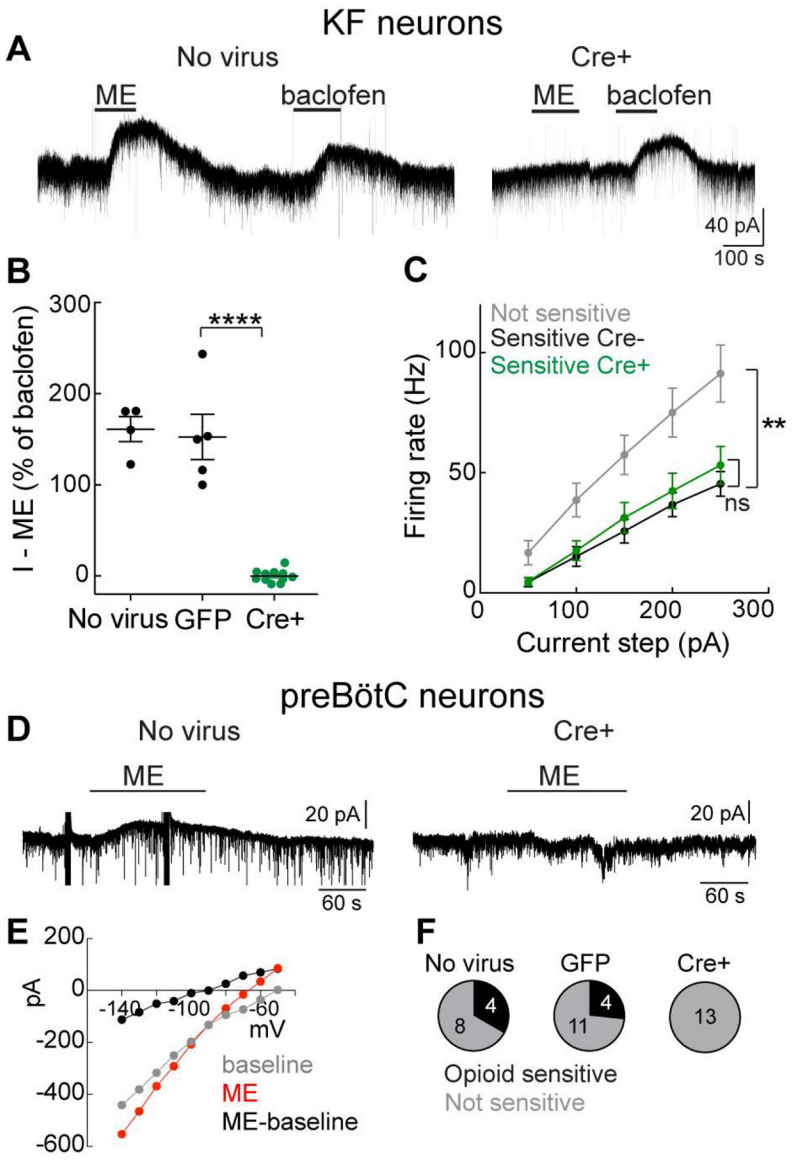

Figure 2. Opioid-mediated currents are abolished from KF and preBötC neurons expressing Cre-GFP.

MOR$^{fl/fl}$ mice were injected with AAV2-CMV-Cre-GFP or AAV2-CMV-GFP into the KF or preBötC. **A**, Whole-cell voltage-clamp recordings from KF neurons in brain slices from MOR$^{fl/fl}$ mice that were naïve (left) or expressing Cre-GFP (right). Opioid agonist [Met^5] -enkephalin (ME, 1 μM) and GABA-B receptor agonist baclofen (30 μM) caused an outward GIRK current in the control, but not Cre-GFP+ neuron. **B**, Summary of the ME-mediated outward current normalized to the baclofen-mediated current. Line and error are mean ± SEM. Individual data points are from individual neurons in a separate slice (one neuron per slice, max of two slices per animal). ****p < 0.0001, by one-way ANOVA and Tukey's post-hoc test. **C**, Current-clamp recordings were made from KF neurons that were opioid/baclofen insensitive (NS), opioid/baclofen sensitive and not expressing Cre-GFP (sensitive Cre-) or opioid/baclofen sensitive and expressing Cre-GFP (sensitive Cre+). Data are mean ± SEM (n = 7–18). **p = 0.0022, ns= not significant by one-way ANOVA and Tukey's post-

hoc test. **D**, Whole-cell voltage-clamp recordings from preBötC neurons in brain slices from $MOR^{fl/fl}$ mice that were naïve (left) or expressing Cre-GFP (right). ME (3 μM) caused an outward current in the control, but not the Cre-GFP+ neuron. Artifact from I-V protocol is present before and during ME. **E**, Example I-V relationship from an ME-sensitive preBötC neuron. Voltage steps (−50 to −140 mV, 50 ms) were performed at baseline (gray) and during ME (3 μM, red). The subtracted I-V is shown in black. **F**, Summary of the proportion of neurons identified with ME currents (opioid sensitive). Numbers within the pie are # of neurons.

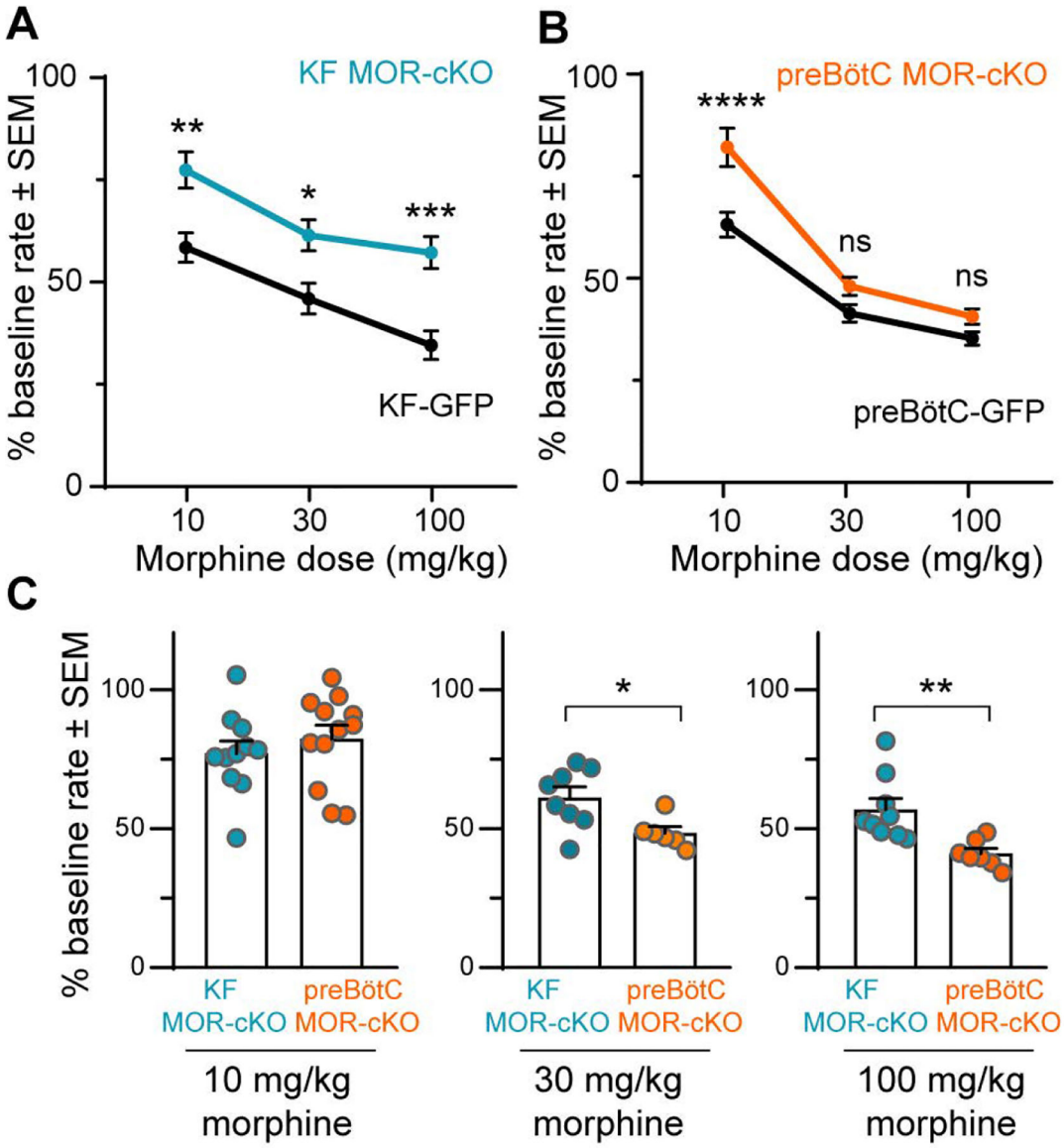

Figure 3. Dose-dependent differential contributions of the KF and preBötC to morphine-induced respiratory rate depression.

Head-out plethysmography in awake adult MOR$^{fl/fl}$ mice expressing GFP or Cre-GFP (MOR-cKO) in KF (**A,C**) or preBötC (**B,C**). Respiratory rate following morphine (10 – 100 mg/kg, ip) was normalized to saline (ip) baseline rate. **A**, KF MOR-cKO mice displayed significantly faster respiratory rates following all doses of morphine. Data are mean ± SEM (n = 6–11). **B**, preBötC MOR-cKO mice had significantly faster respiratory rates following low dose morphine (10 mg/kg). Morphine-induced respiratory depression was similar between GFP and preBötC MOR-cKO mice following 30 mg/kg and 100 mg/kg morphine. Data are mean ± SEM (n = 6–12). *p < 0.05, **p < 0.01, ***p < 0.001, ****p < 0.0001, ns = not significant by one-way ANOVA and Tukey's post-hoc test **C**, Comparison between KF MOR-cKO and preBötC MOR-cKO mice at each morphine dose. Bars are mean ± SEM, individual points are from individual mice. *p < 0.05, **p < 0.01 by unpaired *t*-test.

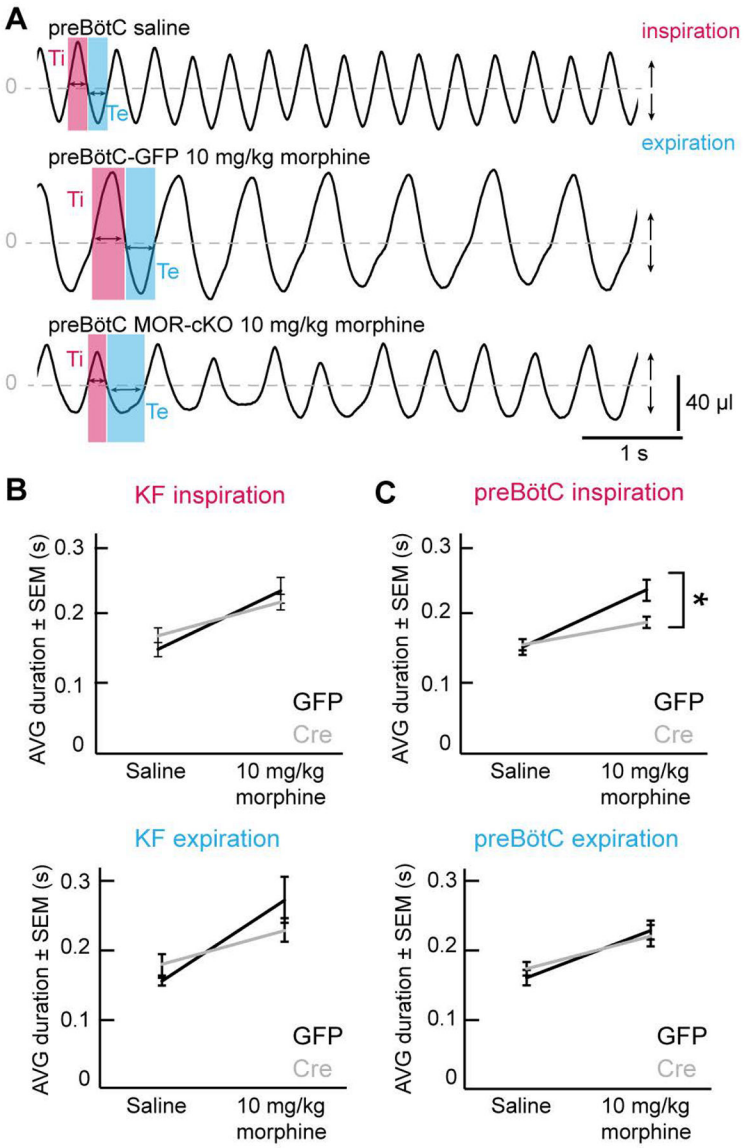

Figure 4. Attenuation of respiratory depression in preBötC MOR-cKO mice is due to changes in inspiration.

A, Example plethysmography traces demonstrating respiratory phases. preBötC-GFP mice displayed regular breathing patterns and stable, ~1:1 ratio inspiratory (T_i) and expiratory (T_e) phases following saline and low dose morphine (10 mg/kg). The inspiratory phase duration was significantly shorter in preBötC MOR-cKO animals following low dose morphine (10 mg/kg). All examples are from the steady-state phase (> 30 min) following morphine or saline injection. **B**, Inspiratory and expiratory phase durations increased proportionately in the KF-GFP control group, as well as the KF MOR-cKO group following morphine (10 mg/kg). Data are mean ± SEM, n = 11. **C**, There was a significant attenuation of the low dose morphine (10 mg/kg)-induced increase in inspiratory duration in preBötC MOR-cKO mice compared to GFP injected controls. Data are mean ± SEM, n = 12. *p<0.05 by unpaired *t*-test.

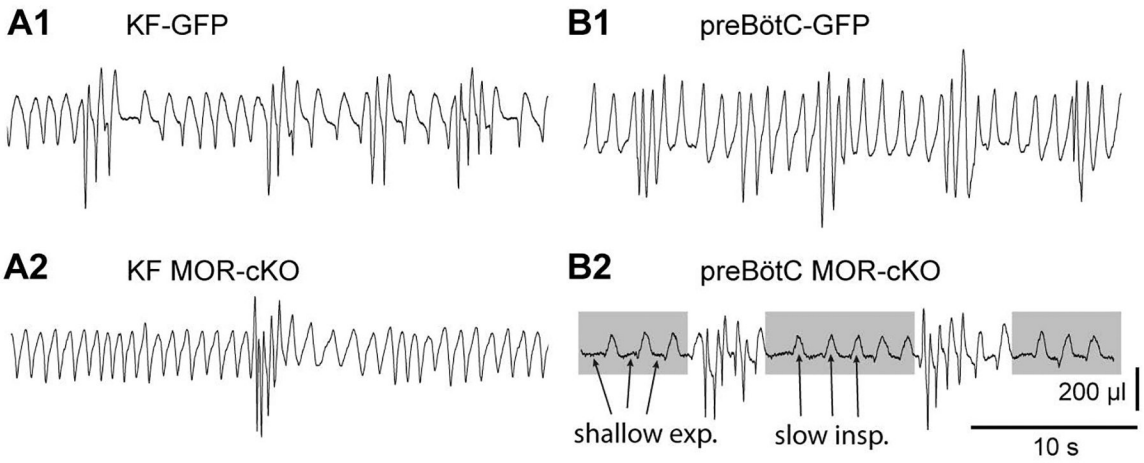

Figure 5. Removal of MORs from the preBötC results in increased variability in the respiratory pattern following high dose morphine.

Example plethysmography traces following high-dose morphine (100 mg/kg, ip) from KF-GFP **(A1)**, KF MOR-cKO **(A2)**, preBötC-GFP mice **(B1)** showing intermixed fast and slow breathing rates with smooth inspiration and expiration phase transitions. **B2**, preBötC MOR-cKO example trace following morphine (100 mg/kg, ip). Gray shaded boxes indicate periods of slow rate, with arrows indicating shallow expiratory periods and triangular inspirations that resemble gasping. Periods of gasping were interrupted by faster, higher amplitude activity.

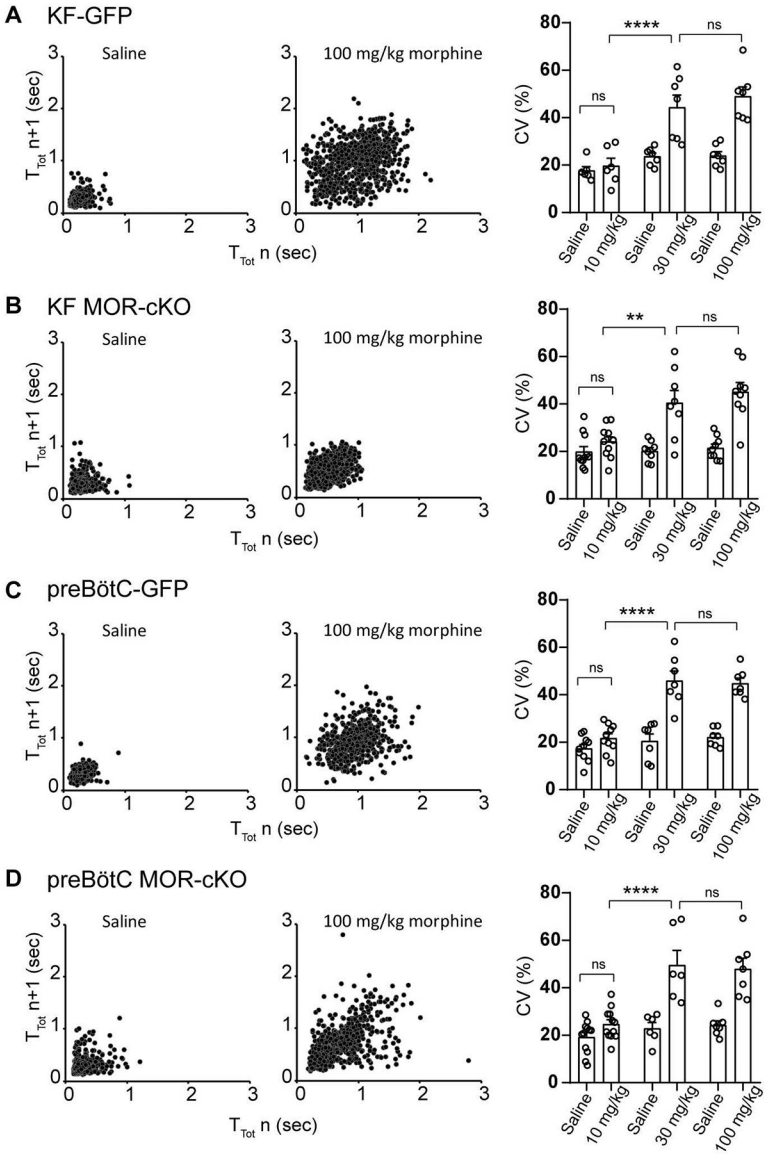

Figure 6. High dose morphine induces irregular breathing patterns.

Left columns, Representative example Poincaré plots of the respiratory cycle duration T_{Tot} for n^{th} cycle versus T_{Tot} for the n^{th} + 1 cycle following saline and 100 mg/kg dose morphine administration for (**A**) KF-GFP, (**B**) KF-MOR-cKO, (**C**) preBötC-GFP and (**D**) preBötC-MOR-cKO groups. Right column, summary bar graphs show that the coefficient of variation (CV %) of instantaneous breathing frequency is significantly higher following 30 mg/kg and 100 mg/kg morphine administration in every group. Between-group comparisons did not reveal statistical differences (GFP vs. MOR-cKO, KF-MOR-cKO vs. preBötC-MOR-cKO). Data are mean ± SEM (n = 6–12). **p < 0.01, ****p < 0.0001, ns = not significant by two-way ANOVA followed by Holm-Sidak post-hoc test.

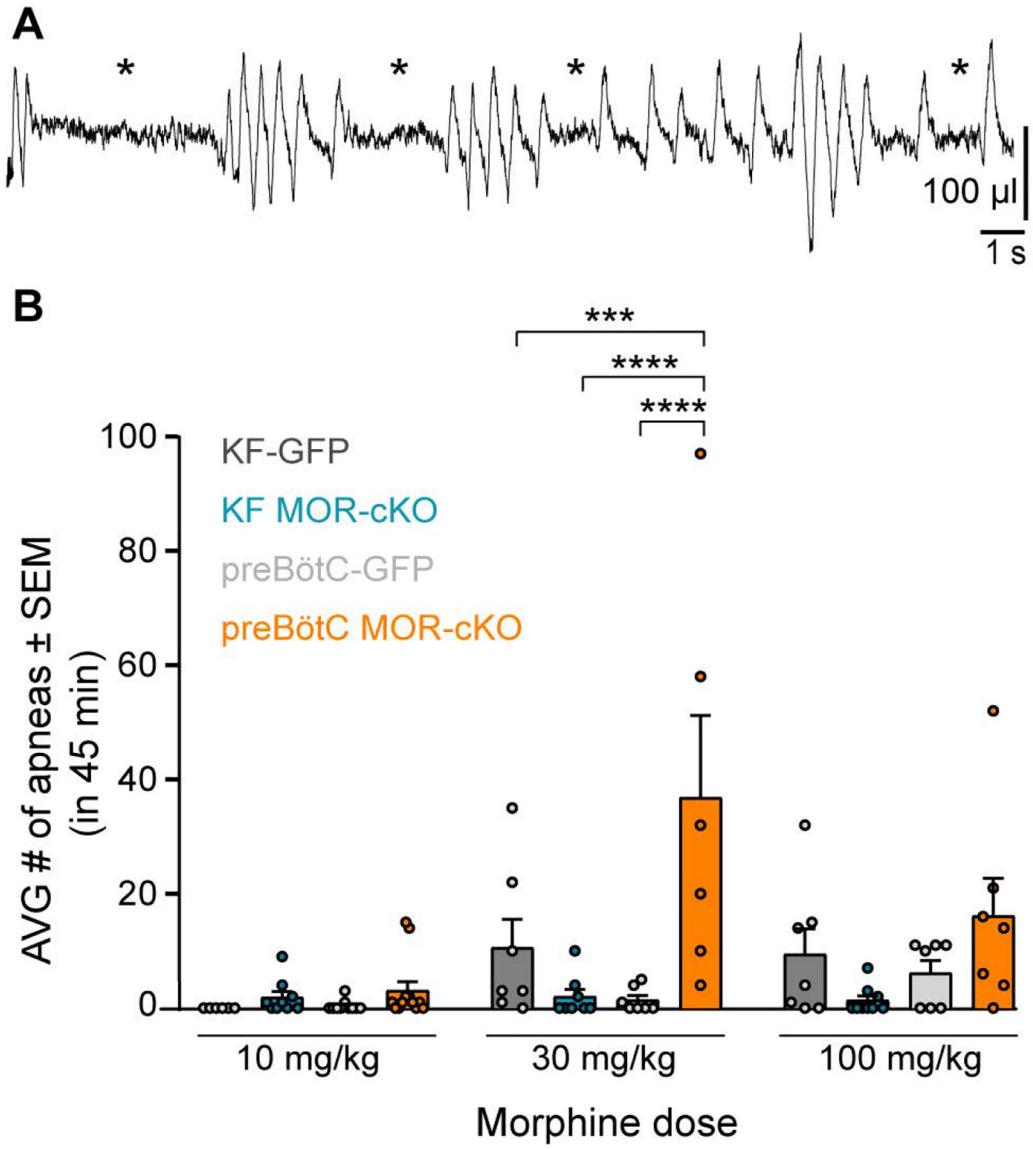

Figure 7. MOR deletion in the preBötC, but not the KF, increases the occurrence of apneas.

A, Example plethysmography trace from a preBötC MOR-cKO animal displaying ataxic breathing patterns with multiple apneas following morphine (100 mg/kg, ip). Apneas are indicated by *. **B**, Summary of the average number of apneas in 45 minutes following morphine (10 – 100 mg/kg). Saline trials (not shown) had 0 – 2 apneas per animal across all groups. Medium (30 mg/kg) dose of morphine induced significantly more apneas in the preBötC MOR-cKO group compared to all groups. No between-group statistical differences were detected for the 10 mg/kg and 100 mg/kg doses. Data are mean ± SEM, individual points are from individual mice, n = 6–12. ***p < 0.001, ****p < 0.0001, by two-way ANOVA and Tukey's post-hoc test.